



HAL
open science

Extension of the lubrication theory for arbitrary wall shape: An asymptotic analysis

Rogers Bill Cordova Hinojosa, Kim Pham, Corinne Rouby

► **To cite this version:**

Rogers Bill Cordova Hinojosa, Kim Pham, Corinne Rouby. Extension of the lubrication theory for arbitrary wall shape: An asymptotic analysis. *Comptes Rendus Mécanique*, 2019, 347 (5), pp.389-396. 10.1016/j.crme.2019.03.016 . hal-02456317

HAL Id: hal-02456317

<https://ensta-paris.hal.science/hal-02456317>

Submitted on 22 Oct 2021

HAL is a multi-disciplinary open access archive for the deposit and dissemination of scientific research documents, whether they are published or not. The documents may come from teaching and research institutions in France or abroad, or from public or private research centers.

L'archive ouverte pluridisciplinaire **HAL**, est destinée au dépôt et à la diffusion de documents scientifiques de niveau recherche, publiés ou non, émanant des établissements d'enseignement et de recherche français ou étrangers, des laboratoires publics ou privés.



Distributed under a Creative Commons Attribution - NonCommercial 4.0 International License

Extension of the lubrication theory for arbitrary wall shape: an asymptotic analysis

R. Cordova H., K. Pham, C. Rouby

IMSIA, CNRS, ENSTA ParisTech, 828 Bd des Maréchaux, 91732 Palaiseau, France

Abstract

We extend the lubrication approximation for a viscous flow in two-dimensional channels with arbitrary shape functions and moderate aspect ratio. The higher-order model is obtained following an asymptotic analysis. Velocity and pressure profiles for the approximated model are given analytically and involve the derivatives of the shape functions of the walls up to the second-order. Comparisons with full-scale simulations are given and show good agreement as well as improvements from the classical standard lubrication approximation.

Keywords: Lubrication approximation, Stokes flow, Asymptotic expansions

1. Introduction

2 The *Classical Lubrication Approximation* (CLA) accounts for the behavior of viscous flows in thin channels under assumptions of small Reynolds numbers and for slowly varying walls. Under these hypotheses, the flow is characterized by (i) a constant pressure across the transverse, say vertical, section and with variations along the channel axis governed by the Reynolds equation [1], (ii) a horizontal **velocity of the Poiseuille's type and a vertical velocity negligible compared to the horizontal velocity.**

9 The CLA, as it avoids to resolve a full-scale fluid calculation, is used in many fields such as film lubricant [2], hydraulic fracture mechanics [3, 4], dykes and sills in volcanism [5], or flows in biological systems such as blood

Email address: kim.pham@ensta-paristech.fr (corresponding author) (K. Pham)

Preprint submitted to Comptes Rendus Mécanique

March 26, 2019

12 cell transport in narrow capillaries [6]. However, its validity as that of the
 13 associated Reynolds equation have to be questioned when the curvature of
 14 the channel is not negligible anymore. A systematic way to do so is to use
 15 asymptotic techniques which are well-adapted due to the small thickness of
 16 the channel compared to the others dimensions. Starting in the 80s, such
 17 *Extended Lubrication Approximation* (ELA) has been applied to channels
 18 with a single wavy wall [7] and with two symmetric wavy walls [8]. In these
 19 references, power series of the stream function have been obtained for low
 20 Reynolds numbers and the results have been applied in hydraulic fracture
 21 mechanics, see *e.g.* [9] and references herein. We also mention the works of
 22 [10] concerning roughnesses for which the asymptotic analysis is combined
 23 to homogenization to extract the macroscopic effective behavior. Recently,
 24 Tavakol and co-workers have revisited the problem of a single wavy wall using
 25 a slightly different approach in which the asymptotic analysis is applied to
 26 the Stokes equations [11]. Experimental and numerical results support their
 27 analytical result and exemplify the interest of the improved model to capture
 28 accurately the velocity profiles and the pressure drop. Our study follows from
 29 this work and extends the lubrication approximation to two non-symmetric
 30 wavy wall.

31 The paper is organized as follows. The problem is introduced in Section 2
 32 along with the main result of the paper. In Section 3, we will proceed to the
 33 derivation of ELA by means of asymptotic techniques. Finally, in Section 4,
 34 we compare the behavior of the second order asymptotic approximation to
 35 direct numerical simulations and to the prediction from the standard lubri-
 36 cation theory.

37 2. Problem setting and main result

We consider an incompressible, steady, two-dimensional pressure-driven
 flow in a channel of length L . The geometry is defined through the intro-
 duction of the upper shape function $y = h_+(x)$ and the lower shape function
 $y = h_-(x)$ for $x \in (0, L)$ with $h_+ > h_-$ (see Fig. 1). These functions are
 assumed to be at least C^2 continuous. We introduce the mean line level y_m
 and the local half-thickness h of the channel defined by

$$y_m = \frac{h_+ + h_-}{2}, \quad h = \frac{h_+ - h_-}{2}, \quad (1)$$

38 both being function of x . We then rescale the vertical coordinate and center
 39 it around the average level according to

$$\mathbf{y} = \frac{y - y_m(x)}{h(x)}. \quad (2)$$

40

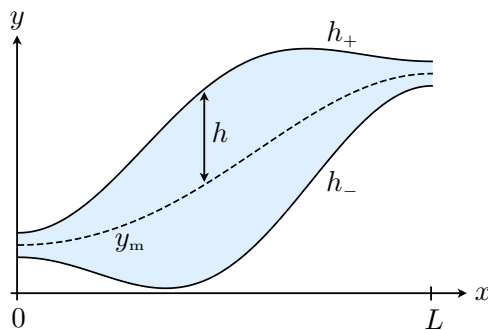


Figure 1: Schematic view of a channel of length L with arbitrary upper and lower shape profiles $h_+(x)$ and $h_-(x)$. The functions $h(x)$ and $y_m(x)$ denote the half-distance between the walls and the average level respectively.

The Reynolds number is assumed to be small so that the flow is governed by the Stokes equations

$$\nabla \cdot \mathbf{u} = 0, \quad \mu \nabla^2 \mathbf{u} = \nabla p, \quad (3)$$

where $\mathbf{u} = u\mathbf{e}_x + v\mathbf{e}_y$ and p are the velocity and the pressure fields respectively, and μ is the viscosity of the fluid. Additionally to a no-slip condition on the walls, the boundary conditions are defined as prescribed a Poiseuille inlet velocity profile and a vanishing outlet pressure

$$\mathbf{u}(x, h_+(x)) = \mathbf{u}(x, h_-(x)) = \mathbf{0}, \quad \mathbf{u}(0, y) = \frac{3\Phi}{4h(0)} (1 - y^2) \mathbf{e}_x, \quad p(L, y) = 0, \quad (4)$$

41 with Φ the fluid flux. To conduct the asymptotic analysis, we define the
 42 small parameter

$$\varepsilon = \frac{h(0)}{L}, \quad (5)$$

which accounts for the slenderness ratio of the channel. The main result of the paper is the following approximation of the exact solution of the problem up to the second order in the small parameter ε

$$u(x, y) = \frac{3\Phi}{4h} (1 - y^2) \left(1 + \frac{4h'^2 - hh''}{10} (1 - 5y^2) + \frac{2hy_m'' - 12h'y_m'}{3} y \right) + u_c o(\varepsilon^2), \quad (6)$$

$$v(x, y) = \frac{3\Phi}{4h} (1 - y^2) (h'y + y_m') + u_c o(\varepsilon^2), \quad (7)$$

$$p(x, y) = \mu\Phi \int_x^L \frac{3}{2h^3} \left(1 + \frac{2}{5} (h'^2 + hh'' + 5y_m'^2) \right) dx' + \frac{3\mu\Phi}{4h^2} (h'(1 - 3y^2) - 2y_m'y) + p_c o(\varepsilon^2), \quad (8)$$

43 where the characteristic velocity u_c and p_c are given by

$$u_c = \frac{\Phi}{2h(0)}, \quad p_c = \frac{\mu\Phi L}{2(h(0))^3}. \quad (9)$$

44 The classical lubrication approximation is obtained from Eqs. (6)-(8) by simply
 45 putting the derivative of y_m and h to zero. Hence, in the standard case,
 46 the velocities and the pressure depend only on the (half) relative distance
 47 h between the walls. Note that the prescribed parabolic inlet velocity profile
 48 Eq. (4) is matched in *average* by the second-order approximation. It is
 49 matched *exactly* if we have simultaneously $y_m' = h' = 0$ and $y_m'' = h'' = 0$.
 50 If not, there is a discontinuity and the approximation is correct far enough
 51 from the inlet while near the inlet, there exists a boundary layer which can be
 52 determined by a *matched* asymptotic expansion of the governing equations.

53 3. Asymptotic analysis

54 3.1. Dimensionless problem and rescaled equations

In order to non-dimensionalize the problem, the following variables are introduced

$$\mathbf{x} = \frac{x}{L}, \quad \mathbf{u}(\mathbf{x}, \mathbf{y}) = \frac{u}{u_c}, \quad \mathbf{v}(\mathbf{x}, \mathbf{y}) = \frac{v}{u_c}, \quad \mathbf{p}(\mathbf{x}, \mathbf{y}) = \frac{p}{p_c}. \quad (10)$$

55 The recentered and rescaled vertical coordinate, defined by Eq. (2), reads
 56 now

$$\mathbf{y} = \frac{y - h(0)y_m(\mathbf{x})}{h(0)h(\mathbf{x})}, \quad (11)$$

where

$$y_m(\mathbf{x}) = \frac{y_m(L\mathbf{x})}{h(0)}, \quad \mathbf{h}(\mathbf{x}) = \frac{h(L\mathbf{x})}{h(0)}, \quad (12)$$

57 denote the rescaled shape functions that define the channel's geometry.

Introducing the dimensionless differential operators

$$\hat{\partial}_x = \partial_x - \frac{\mathbf{h}'\mathbf{y} + \mathbf{y}'_m}{\mathbf{h}} \partial_y, \quad \hat{\partial}_y = \frac{1}{\mathbf{h}} \partial_y, \quad \hat{\partial}_{yy} = \frac{1}{\mathbf{h}^2} \partial_{yy}, \quad (13)$$

58

$$\hat{\partial}_{xx} = \partial_{xx} + \frac{(\mathbf{h}'\mathbf{y} + \mathbf{y}'_m)^2}{\mathbf{h}^2} \partial_{yy} - 2\frac{\mathbf{h}'\mathbf{y} + \mathbf{y}'_m}{\mathbf{h}} \partial_{xy} + \left(\frac{2\mathbf{h}'(\mathbf{h}'\mathbf{y} + \mathbf{y}'_m)}{\mathbf{h}^2} - \frac{\mathbf{h}''\mathbf{y} + \mathbf{y}''_m}{\mathbf{h}} \right) \partial_y, \quad (14)$$

where ∂_x and ∂_y are the usual derivatives with respect to \mathbf{x} and \mathbf{y} respectively, the Stokes equations read in non dimensional form as

$$\hat{\partial}_x \mathbf{u} + \frac{1}{\varepsilon} \hat{\partial}_y \mathbf{v} = 0, \quad (15)$$

$$\hat{\partial}_{xx} \mathbf{u} + \frac{1}{\varepsilon^2} \hat{\partial}_{yy} \mathbf{u} = \frac{1}{\varepsilon^2} \hat{\partial}_x \mathbf{p}, \quad (16)$$

$$\hat{\partial}_{xx} \mathbf{v} + \frac{1}{\varepsilon^2} \hat{\partial}_{yy} \mathbf{v} = \frac{1}{\varepsilon^3} \hat{\partial}_y \mathbf{p}. \quad (17)$$

These equations are written in the rescaled region $(0, 1) \times (-1, 1)$, and are complemented by the boundary conditions

$$\mathbf{u}(0, y) = \frac{3}{2} (1 - y^2), \quad \mathbf{v}(0, y) = \mathbf{u}(x, \pm 1) = \mathbf{v}(x, \pm 1) = 0, \quad \mathbf{p}(1, y) = 0. \quad (18)$$

59

Next, we follow an asymptotic approach, valid for small ε , in which we assume that the solution $(\mathbf{u}, \mathbf{v}, \mathbf{p})$ can be expanded in powers of ε , namely

$$\mathbf{u}(\mathbf{x}, y) = \sum_{i=0}^{\infty} \varepsilon^i \mathbf{u}_i(\mathbf{x}, y), \quad \mathbf{v}(\mathbf{x}, y) = \sum_{i=0}^{\infty} \varepsilon^i \mathbf{v}_i(\mathbf{x}, y), \quad \mathbf{p}(\mathbf{x}, y) = \sum_{i=0}^{\infty} \varepsilon^i \mathbf{p}_i(\mathbf{x}, y). \quad (19)$$

60 The fields $(\mathbf{u}_i, \mathbf{v}_i, \mathbf{p}_i)$ will be determined by inserting expressions (19) in
61 Eqs. (15)-(18).

62 *3.2. Correction to CLA in the vertical velocity \mathbf{v}_1*

63 To begin with, we shall see that the analysis of the problem at the leading
 64 orders provides the standard Reynolds equation within CLA, corrected by
 65 a non vanishing vertical velocity. Introducing expressions (19) in Eqs. (15)-
 66 (18), we firstly examine the dominant order terms. The continuity equa-
 67 tion (15) reads as $\hat{\partial}_y \mathbf{v}_0 = 0$, which leads to

$$\mathbf{v}_0 = 0, \quad (20)$$

68 because of the no-slip conditions $\mathbf{v}_0(\mathbf{x}, \pm 1) = 0$. The momentum balance
 69 along y (17) gives $\hat{\partial}_y \mathbf{p}_0 = 0$, so that \mathbf{p}_0 is independent of y and we set
 70 $\mathbf{p}_0 = \bar{\mathbf{p}}_0(\mathbf{x})$. The momentum balance along x (16) then reads as $\hat{\partial}_{yy} \mathbf{u}_0 =$
 71 $\partial_x \bar{\mathbf{p}}_0(\mathbf{x})$, which can be integrated with respect to y using the no-slip bound-
 72 ary conditions $\mathbf{u}_0(\mathbf{x}, \pm 1) = 0$. This gives the classical parabolic shape for the
 73 longitudinal velocity at the dominant order

$$\mathbf{u}_0(\mathbf{x}, y) = -\frac{h^2}{2} \partial_x \bar{\mathbf{p}}_0 (1 - y^2). \quad (21)$$

74

75 At the next order, the continuity equation (15) reads as

$$\hat{\partial}_x \mathbf{u}_0 + \hat{\partial}_y \mathbf{v}_1 = 0. \quad (22)$$

76 By integrating this equation with respect to y over $(-1, 1)$, we obtain the
 77 standard Reynolds equation

$$\partial_x \left(-\frac{2}{3} h^3 \partial_x \bar{\mathbf{p}}_0 \right) = 0, \quad (23)$$

78 where we used the expression of \mathbf{u}_0 (21) and the no-slip boundary conditions
 79 $\mathbf{v}_1(\mathbf{x}, \pm 1) = 0$. This shows us that the rescaled flux

$$\phi_0 = -\frac{2}{3} h^3 \partial_x \bar{\mathbf{p}}_0, \quad (24)$$

80 is a quantity conserved along the channel. Comparing the boundary condi-
 81 tions $\mathbf{u}_0(0, y) = \frac{3}{2} (1 - y^2)$ to Eq. (21) provides $\phi_0 = 2$. Finally, the longitu-
 82 dinal velocity at the dominant order reads as

$$\mathbf{u}_0(\mathbf{x}, y) = \frac{3}{2h} (1 - y^2). \quad (25)$$

83 The pressure \bar{p}_0 in the channel can now be deduced by integration of Eq. (24).
 84 Given the boundary condition $p_0(1, y) = 0$, we get

$$p_0(x, y) = \bar{p}_0(x) = \int_x^1 \frac{3}{h^3} dx'. \quad (26)$$

85

86 We are now able to derive the first non-trivial contribution to the vertical
 87 velocity. Since u_0 is known from Eq. (25), the continuity equation (22) can
 88 be integrated with respect to y , which leads to the first correction to CLA in
 89 the vertical velocity

$$v_1(x, y) = \frac{3}{2} (1 - y^2) \frac{h'y + y'_m}{h}. \quad (27)$$

90 *3.3. Extended lubrication approximation and corrections in (u_2, p_2)*

We shall now complement the correction in the vertical velocity obtained above by deriving the correction in the pressure and the associated horizontal velocity. To achieve this, we examine the terms of higher orders in Eqs. (15)-(17). Because of $v_0 = 0$, the terms p_1 , u_1 and v_2 satisfy the same relations as at lower order, namely

$$\hat{\partial}_x u_1 + \hat{\partial}_y v_2 = 0, \quad \hat{\partial}_{yy} u_1 = \hat{\partial}_x p_1, \quad \hat{\partial}_y p_1 = 0. \quad (28)$$

This provides the same result, with $p_1(x, y) = \bar{p}_1(x)$, $u_1(x, y) = \frac{h^2}{2} \partial_x \bar{p}_1 (y^2 - 1)$ and the flux $\phi_1 = -\frac{2}{3} h^3 \partial_x \bar{p}_1$ conserved along x . However the boundary conditions (18), by means of the prescribed inlet velocity $u_1(x, 0) = 0$ and pressure at the exit $p_1(1, y) = 0$, imply $\phi_1 = 0$ and

$$u_1(x, y) = 0, \quad p_1(x, y) = 0. \quad (29)$$

91 Integrating the continuity equation at this order leads to

$$v_2(x, y) = 0. \quad (30)$$

The pursuit of the analysis at the next order is necessary to reveal new contributions from Eqs. (15)-(17). Specifically, we now start with

$$\hat{\partial}_x u_2 + \hat{\partial}_y v_3 = 0, \quad \hat{\partial}_{xx} u_0 + \hat{\partial}_{yy} u_2 = \hat{\partial}_x p_2, \quad \hat{\partial}_{yy} v_1 = \hat{\partial}_y p_2. \quad (31)$$

92 Given the non trivial value (27) of \mathbf{v}_1 , the pressure \mathbf{p}_2 is deduced, up to a
 93 constant of \mathbf{x} , by integrating the third equation of (31). We obtain

$$\mathbf{p}_2(\mathbf{x}, \mathbf{y}) = \bar{\mathbf{p}}_2(\mathbf{x}) + \frac{3}{2h^2} (h' (1 - 3y^2) - 2y'_m y), \quad (32)$$

where $\bar{\mathbf{p}}_2(\mathbf{x})$ is the average of \mathbf{p}_2 over $\mathbf{y} \in (-1, 1)$. The longitudinal velocity \mathbf{u}_2 is then calculated thanks to the second equation of (31). Plugging the forms of \mathbf{u}_0 and \mathbf{p}_2 from Eqs. (25) and (32) into this equation leads to

$$\begin{aligned} \partial_{yy} \mathbf{u}_2 = & -\frac{3}{h} \left(hh'' (3y^2 - 1) + 2h'^2 (1 - 6y^2) - 2y'_m{}^2 + 2(hy''_m - 6h'y'_m) y \right) \\ & + h^2 \hat{\partial}_x \bar{\mathbf{p}}_2. \end{aligned} \quad (33)$$

94 The integration of this expression, taken into account the no-slip conditions
 95 $\mathbf{u}_2(\mathbf{x}, \pm 1) = 0$, provides \mathbf{u}_2 of the form

$$\mathbf{u}_2(\mathbf{x}, \mathbf{y}) = 3(1 - y^2) \left[\frac{hh'' - 4h'^2}{4h} y^2 - \frac{hh'' + y'_m{}^2}{4h} + \left(\frac{y''_m}{3} - \frac{2h'y'_m}{h} \right) y - \frac{h^2}{6} \hat{\partial}_x \bar{\mathbf{p}}_2 \right], \quad (34)$$

96 with $\hat{\partial}_x \bar{\mathbf{p}}_2$ still unknown at this stage. In order to determine this term, the first
 97 equation of (31) is integrated over $\mathbf{y} \in (-1, 1)$, which leads to $\int_{-1}^1 \hat{\partial}_x \mathbf{u}_2 \, d\mathbf{y} = 0$
 98 because of the no-slip conditions $\mathbf{v}_3(\mathbf{x}, \pm 1) = 0$, and eventually

$$h^3 \hat{\partial}_x \bar{\mathbf{p}}_2 = -\frac{6}{5} (hh'' + h'^2 + 5y'_m{}^2). \quad (35)$$

99 Finally, plugging the above expression into Eq. (34) leaves us with

$$\mathbf{u}_2(\mathbf{x}, \mathbf{y}) = \frac{3}{2h} (1 - y^2) \left(\frac{4h'^2 - hh''}{10} (1 - 5y^2) + \frac{2hy''_m - 12h'y'_m}{3} y \right). \quad (36)$$

100 The pressure $\bar{\mathbf{p}}_2$ is obtained by integrating Eq. (35) with the boundary con-
 101 dition $\bar{\mathbf{p}}_2(1) = 0$, which gives

$$\bar{\mathbf{p}}_2(\mathbf{x}) = \int_{\mathbf{x}}^1 \frac{6}{5h^3} (h'^2 + hh'' + 5y'_m{}^2) \, d\mathbf{x}'. \quad (37)$$

102 3.4. Reconstruction of the solution

By adding the contributions at each order (Eqs. (25), (29) and (36) for \mathbf{u} ; Eqs. (20), (27) and (30) for \mathbf{v} ; Eqs. (26), (29) and (32) along with (37) for

ρ), we reconstruct an approximation of the solution $(\mathbf{u}, \mathbf{v}, \rho)$ up to the second order in ε . In dimensionless form, this gives us

$$\mathbf{u} = \frac{3}{2h}(1 - y^2) \left[1 + \varepsilon^2 \left(\frac{4h'^2 - hh''}{10}(1 - 5y^2) + \frac{2hy''_m - 12h'y'_m y}{3} \right) \right] + o(\varepsilon^2), \quad (38)$$

$$\mathbf{v} = \frac{3\varepsilon}{2h}(1 - y^2)(h'y + y'_m) + o(\varepsilon^2), \quad (39)$$

$$\begin{aligned} \rho = \int_x^1 \frac{3}{h^3} \left(1 + \frac{2\varepsilon^2}{5} (h'^2 + hh'' + 5y_m'^2) \right) dx' \\ + \frac{3\varepsilon^2}{2h^2} (h'(1 - 3y^2) - 2y'_m y) + o(\varepsilon^2), \end{aligned} \quad (40)$$

103 which, coming back to the dimensional parameters defined by Eq. (10), gives
104 the form announced in Eqs. (6)-(8).

105 4. Validation of the ELA model

To inspect the accuracy of the ELA model specified by Eqs. (6)-(8), we consider two channel's profiles (P1) and (P2) where both y_m and h vary. The geometries of the channels, of length $L = 1$, are defined by the following equations:

$$(P1) \begin{cases} h_+(x) = 0.2 \cos(\pi(x - 1/2))^2 + 0.2, \\ h_-(x) = \frac{1}{3} \cos(\pi(x - 1/2))^2, \end{cases} \quad (41)$$

$$(P2) \begin{cases} h_+(x) = 0.15 \cos(\pi(x - 1/2))^2 + 0.1 + 0.35 \cos(\pi(x/2 - 1/2))^2, \\ h_-(x) = -0.2 \cos(\pi(x - 1/2))^2 + 0.05 + 0.35 \cos(\pi(x/2 - 1/2))^2. \end{cases} \quad (42)$$

106 These profiles are represented in Fig. 2.

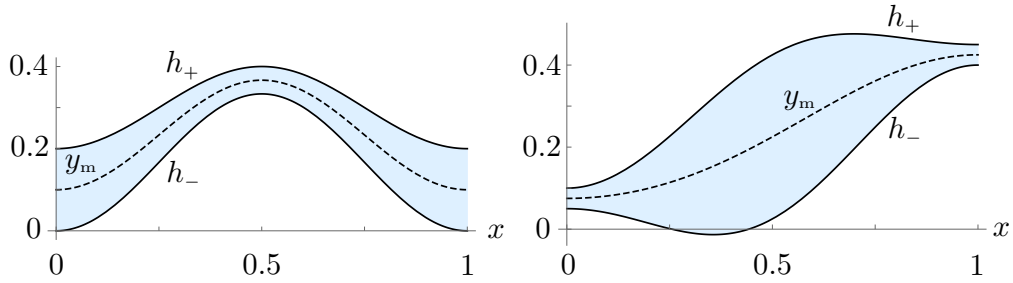


Figure 2: Profiles used for the comparisons with the full scale simulations: (left) channel's profile (P1), (right) channel's profile (P2).

107 For (P1) and (P2), we have $h'_+(0) = h'_-(0) = 0$ and $h'_+(1) = h'_-(1) = 0$.
 108 The prescribed inlet velocity (4) is chosen such that the flux is $\Phi = 1$ and the
 109 fluid viscosity is set at $\mu = 1$. We use COMSOL to solve the direct problem
 110 (3) along with the boundary conditions (4).

111 We report in Figs. 3, 4 and 5 the fields of the velocity components (u, v)
 112 and of the pressure p computed numerically and the corresponding fields
 113 predicted by the CLA and ELA; for the CLA, $v(x, y) = 0$ is not shown.

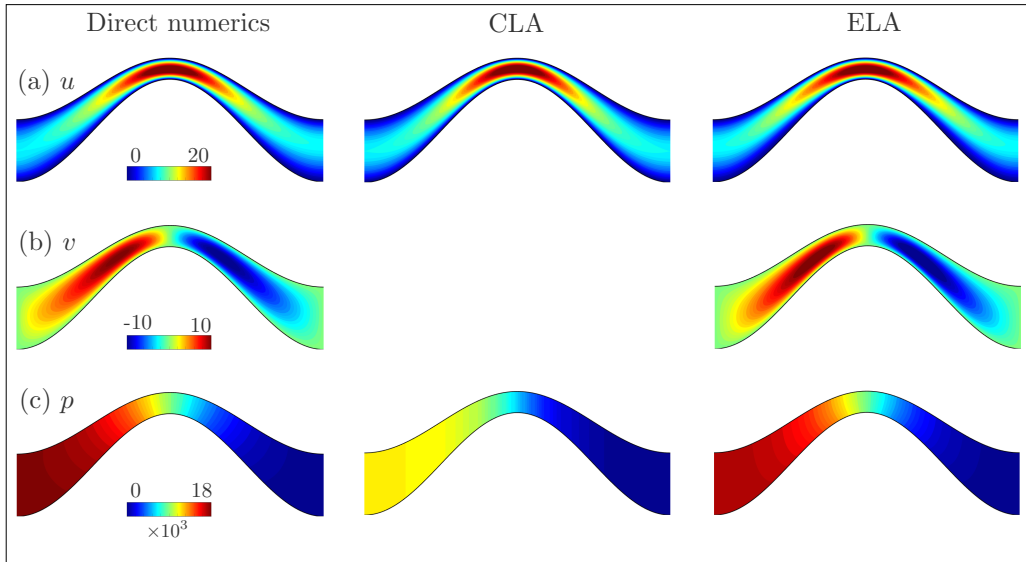


Figure 3: Results for the profile (P1). Fields of the velocity components (u, v) and of the pressure p in full scale simulations, CLA and ELA.

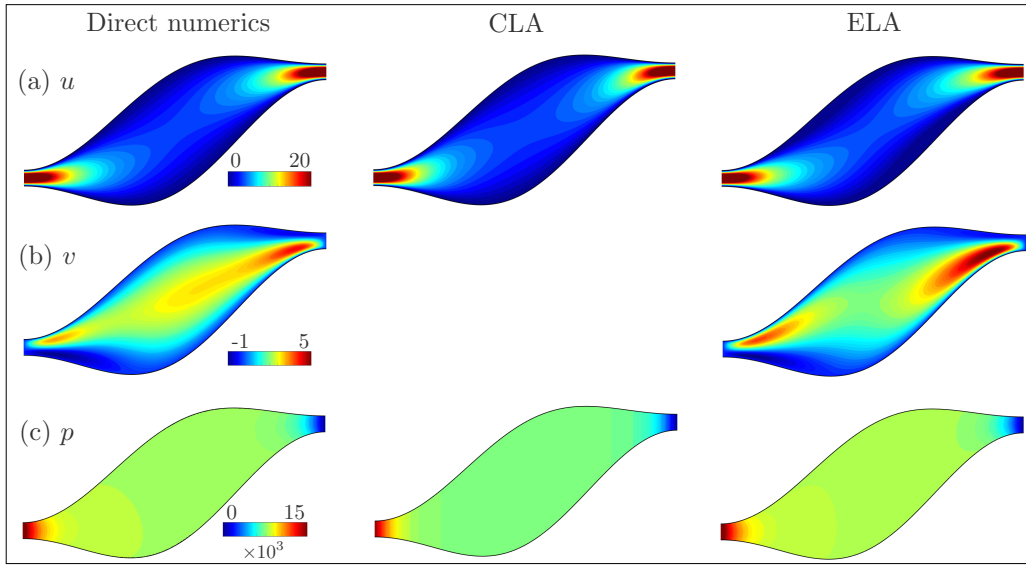


Figure 4: Results for the profile (P2). Same representation as in Fig. 3.

Profile	$\max(2h)$	h'	h''	y'_m	y''_m
(P1)	0.2	~ 0.2	~ 1	~ 1	~ 5
(P2)	0.4	~ 0.5	~ 3	~ 0.5	~ 2

Table 1: Typical values of the characteristics of the profiles chosen for the comparison

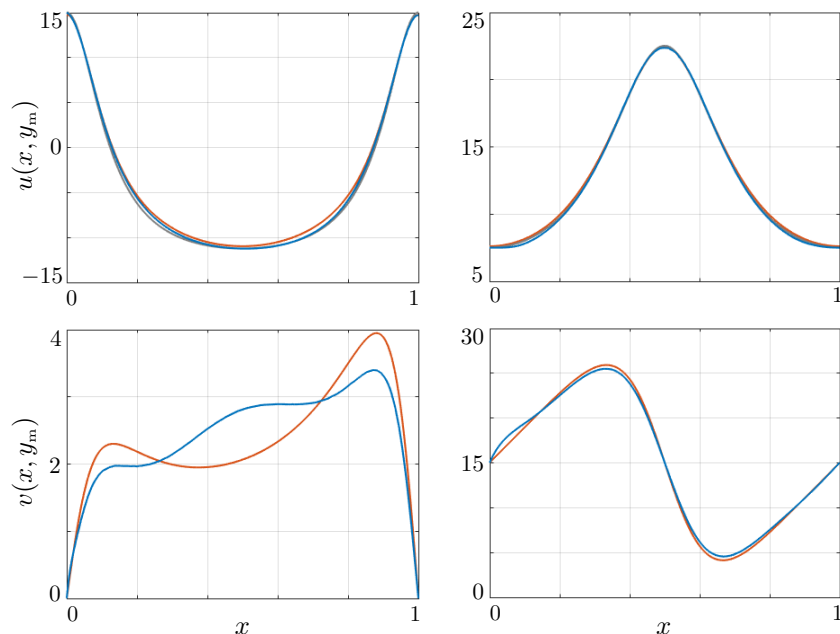


Figure 5: Variations of the horizontal velocity $u(x, y_m)$ and vertical velocity $v(x, y_m)$ with respect to x , calculated at the centerline $y = y_m$. Red line shows the velocity field computed numerically, blue line shows the prediction in ELA from (8); grey line shows the horizontal velocity in CLA (we do not represent the vertical velocity as it is neglected in CLA).

114 In the reported cases, the profiles have the characteristics given in Table 1.
115 The two channels have a reasonable small slenderness ratio $\max(2h)$ as well
116 as moderate slopes/curvatures which do not exceed few unities. Besides
117 they produce flows with similar maximum horizontal velocities and similar
118 pressure drops. However, the improvement of ELA compared to CLA is
119 much more impressive for (P1) than for (P2) and we shall see that this is
120 attributable to more significant slopes y'_m of the centerline, a parameter which
121 is not related to the slenderness ratio. Hence, even though (P1) has a smaller
122 slenderness ratio, the deviation of the flow characteristics with respect to the

123 CLA prediction is more significant, and interestingly, the asymptotic analysis
 124 appears to be more robust with respect to large centerline slopes than to large
 125 slenderness ratio.

126 To begin with, it is noticeable that CLA and ELA have the same good
 127 accuracy to capture the right variations of $u(x, y)$ and this is expected since
 128 the correction δu of ELA appears at the second order. From Eq. (6), this
 129 correction near the centerline varies as $\delta u \sim (4h'^2 - hh'')/10 \sim 0.01$ in
 130 the reported cases. Accordingly, we find an error averaged on the whole
 131 channel of about 2% for (P1) and 4% for (P2). The effect on the vertical
 132 velocity $v(x, y)$ is much more significative and again this is expected since
 133 the correction appears at the first order. But in this case, from Eq. (7), v
 134 is crucially dependent on y'_m , since $v/u \sim y'_m$ near the centerline. It results
 135 that the large slope of the mean line in (P1) close to unity produces vertical
 136 velocities up to half the horizontal one.

137 We now move on to the fields of pressure, which are of particular interest
 138 since the pressure drop due to expansions/constrictions are important in
 139 many practical situations. As for the vertical velocity, the gain in the ELA is
 140 more impressive for (P1) than for (P2) although the slenderness ratio of the
 141 former is half that of the latter: for (P1), the error between the prediction
 142 and the direct numerics is of about 5% for ELA while this error is of about
 143 40% for CLA; for (P2) the error is of 1% for ELA versus 10% for CLA. To
 144 better understand the influence of the different parameters in the ELA, we
 145 define $p_{\text{CLA}}(x) = \mu\Phi \int_x^L 3/(2h^3)dx'$ as the pressure predicted by the CLA;
 146 from Eq. (8), the ELA involves two corrections compared to the CLA

$$p(x, y) = p_{\text{CLA}}(x) + \delta\bar{p}(x) + \delta p(x, y), \quad (43)$$

with

$$\delta\bar{p} = \mu\Phi \int_x^L \frac{3}{5h^3} \left(h'^2 + hh'' + 5y'_m{}^2 \right) dx', \quad \delta p = \frac{3\mu\Phi}{4h^2} \left(h'(1 - 3y^2) - 2y'_m y \right).$$

147 The term δp tells us that the isolines of pressure are not vertical and its
 148 relative weight $\delta p/p_{\text{CLA}} \sim hh'/L$ is given by the slenderness ratio, hence here
 149 negligible. Conversely, the term $\delta\bar{p}$ is an integral along x (as p_{CLA}) and as
 150 such it cumulates the effects of slopes and curvatures. Its weight contains
 151 a contribution in $\int y'_m{}^2/h^3$ which becomes significant when large variations
 152 of the centerline coincide with small slenderness. This happens for (P1) but

153 not for (P2) and the consequences are shown in Fig. 6 where we reported the
 154 pressure profiles $p(x, h_{\pm})$ along the channel walls computed numerically, and
 155 the CLA and ELA predictions. For (P1) the actual pressure drop, $\bar{p}(0) \sim$
 156 18.10^3 , is correctly predicted by ELA while largely underestimated by CLA.
 157 In contrast the gain for (P2) in ELA is moderate compared to CLA.

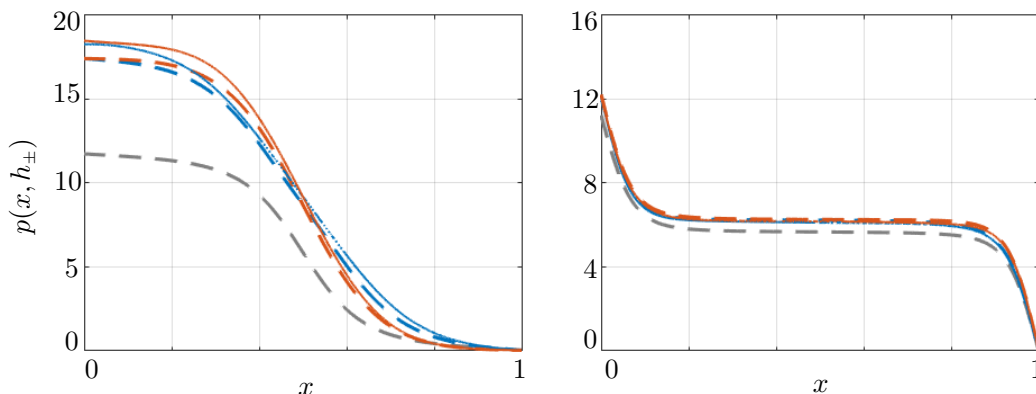


Figure 6: Variations of the pressure with respect to x . Plain lines show the pressure profiles $p(x, h_{\pm})$ computed numerically (blue at $y = h_+$, red at $y = h_-$), dotted lines show the prediction in ELA from (8); dashed grey lines show $p(x, y) = p_{\text{CLA}}(x)$ being independent of y in CLA.

158 5. Conclusion

159 We have derived in this paper a second-order lubrication approximation
 160 for viscous flow at low Reynolds number in thin channels with arbitrary
 161 walls shape. Velocities and pressure profiles in the channel have been given
 162 as fully explicit functions of the inlet flux and the walls geometry, up to
 163 the second derivative. The resulting ELA is in general better than the CLA
 164 and this has been exemplified by comparison with direct numerics. However,
 165 there are situations where the CLA fails in accurate predictions although
 166 the criterion of small slenderness ratio is met. These situations corresponds
 167 to channels containing constrictions coinciding with large variations of the
 168 centerline. This results in large vertical velocities and pressure drops largely
 169 underestimated by CLA and accurately reproduced by ELA.

170 Extension of the current work deals with the derivation of similar higher-
171 order lubrication approximation for (i) moderate (yet non-negligible) Rey-
172 nolds number, starting from the full Navier-Stokes equation, (ii) non station-
173 ary case with time varying walls.

174 6. References

- 175 [1] O. Reynolds, On the theory of lubrication and its application to mr.
176 beauchamp towers experiments, including an experimental determina-
177 tion of the viscosity of olive oil, Philosophical Transactions of the Royal
178 Society of London 177 (1886) 157–234.
- 179 [2] B. J. Hamrock, S. R. Schmid, B. O. Jacobson, Fundamentals of fluid
180 film lubrication, CRC press, 2004.
- 181 [3] E. Detournay, Propagation regimes of fluid-driven fractures in imper-
182 meable rocks, International Journal of Geomechanics 4 (2004) 35–45.
- 183 [4] B. Taisne, S. Tait, C. Jaupart, Conditions for the arrest of a vertical
184 propagating dyke, Bulletin of Volcanology 73 (2011) 191–204.
- 185 [5] J. R. Lister, Buoyancy-driven fluid fracture: similarity solutions for
186 the horizontal and vertical propagation of fluid-filled cracks, Journal of
187 Fluid Mechanics 217 (1990) 213–239.
- 188 [6] Y. Aboelkassem, A. Staples, A bioinspired pumping model for flow in a
189 microtube with rhythmic wall contractions, J. Fluid. Struct. 42 (2013)
190 187–204.
- 191 [7] E. Hasegawa, H. Izuchi, On steady flow through a channel consisting of
192 an uneven wall and a plane wall: Part 1. case of no relative motion in
193 two walls, Bulletin of JSME 26 (1983) 514–520.
- 194 [8] M. Van Dyke, Slow variations in continuum mechanics, in: Advances
195 in applied mechanics, volume 25, Elsevier, 1987, pp. 1–45.
- 196 [9] S. Sisavath, A. Al-Yaarubi, C. C. Pain, R. W. Zimmerman, A simple
197 model for deviations from the cubic law for a fracture undergoing dila-
198 tion or closure, in: Thermo-Hydro-Mechanical Coupling in Fractured
199 Rock, Springer, 2003, pp. 1009–1022.

- 200 [10] J. Fabricius, Y. Koroleva, A. Tsandzana, P. Wall, Asymptotic behaviour
201 of Stokes flow in a thin domain with a moving rough boundary, Proc.
202 R. Soc. A 470 (2014) 20130735.
- 203 [11] B. Tavakol, G. Froehlicher, D. P. Holmes, H. A. Stone, Extended lu-
204 brication theory: improved estimates of flow in channels with variable
205 geometry, Proc. R. Soc. A 473 (2017) 20170234.